Applied Catalysis B: Environmental 123–124 (2012) 440–447

Contents lists available at SciVerse ScienceDirect

Applied Catalysis B: Environmental

journal homepage: www.elsevier.com/locate/apcatb

Synthesis of flower-like Co_3O_4–CeO_2 composite oxide and its application to catalytic degradation of 1,2,4-trichlorobenzene

Shijing Lin[a,b], Guijin Su[a], Minghui Zheng[a,*], Dekun Ji[b], Manke Jia[a], Yexuan Liu[a]

[a] State Key Laboratory of Environmental Chemistry and Ecotoxicology, Research Center for Eco-environmental Sciences, Chinese Academy of Sciences, P.O. Box 2871, Beijing 100085, China

[b] Department of Chemical Engineering, Beijing Institute of Petrochemical Technology, Beijing 102617, China

ARTICLE INFO

Article history:
Received 7 December 2011
Received in revised form 8 May 2012
Accepted 10 May 2012
Available online 17 May 2012

Keywords:
Micro/nano composite material
1,2,4-Trichlorobenzene
Catalytic degradation
Synergistic effect
Apparent activation energy

ABSTRACT

A micrometer-sized, nanostructured, flower-like Co_3O_4–CeO_2 composite oxide was synthesized by an ethylene-glycol-mediated process. The composite oxide was an assembly of polycrystalline nanoparticles, with a typical mesoporous structure. The composite's catalytic activity in 1,2,4-trichlorobenzene degradation was evaluated using a pulsed-flow microreactor–gas chromatography system, and compared with that of quartz sand, commercial CeO_2, commercial Co_3O_4, and a Co_3O_4/CeO_2 equimass mixture. The composite oxide was a promising catalyst for 1,2,4-trichlorobenzene degradation. This is attributed to the structural features of the composite oxide with a high specific surface area and a high total pore volume, and the synergistic effect between the two composite phases. The easy creation of high-mobility active oxygen on CeO_2 and the easy cleavage of Co—O bonds at the interface of the two components promote reactivity of Co_3O_4 in 1,2,4-trichlorobenzene degradation. Pulsed catalytic theory suggests a first-order reaction between the composite oxide and 1,2,4-trichlorobenzene, with an apparent activation energy of about 27 kJ/mol, and degradation on the Co_3O_4–CeO_2 composite oxide would occur easily.

1. Introduction

Cobalt-oxide-based materials have been identified as preferred catalysts for environmental protection processes such as the abatement of CO [1,2], N_2O decomposition [3,4], and phenol degradation [5]. Recently, these materials have been widely investigated with the aim of improving their catalytic properties [6]. In this context, the combination of cobalt oxides with other metal oxides has attracted much attention, especially combinations with rare-earth metal oxides. Multicomponent materials can provide novel multifunctionalities that the single components do not have, and then enhance their performance [7]. CeO_2, a typical rare-earth oxide, is used as a promoter additive because of its high oxygen-storage and oxygen-releasing capacities [8]. Combinations of Co_3O_4 with CeO_2 have been used in many processes such as methane oxidation [9], N_2O decomposition [10], diesel-soot oxidation [11], and low-temperature CO oxidation [8,12,13]. In these reactions, the catalytic performance of Co_3O_4 is greatly improved by the addition of CeO_2 because of a synergistic catalytic effect. Catalysts consisting of cobalt and cerium oxides have therefore been the subject of intense interest [13].

Catalytic activity significantly depends on the catalyst's structural properties such as morphology, surface area, component dispersion, and interaction strength between components. In turn, these structural properties are often determined by the preparation methods [13,14]. Therefore, a wealth of methods has been developed for controlled synthesis of hierarchically nanostructured materials [15–22]. Recently, an ethylene-glycol-mediated process, based on a simple and economical route, has been used to successfully synthesize three-dimensional (3D) micro/nano materials [23–29]. 3D micro/nano materials are often hierarchically composed of nanosized building blocks, and the particle size is on the micrometer scale. Since the composite structure is made up of interconnected nanoparticles, the specific surface area can remain relatively large. Moreover, this hierarchical structure can effectively inhibit aggregation, and thus retain high activity, because the particles are micrometer-sized, and their separation and recycling are easier than in the case of common nanoparticles. Micro/nano materials are therefore promising candidates for many applications [25]. Fabricating a 3D micro/nano Co_3O_4–CeO_2 (Co–Ce) composite oxide would therefore improve the catalytic performance of the composite oxide. Although many single metal oxides with 3D micro/nano structures have been successfully synthesized [23–29], there have been few reports of the synthesis of 3D micro/nano multicomponent metal-oxide materials [7]. The synthesis of a 3D micro/nano Co–Ce composite oxide is therefore a challenge.

* Corresponding author. Tel.: +86 10 62849172; fax: +86 10 62923563.
E-mail address: zhengmh@rcees.ac.cn (M. Zheng).

0926-3373/$ – see front matter © 2012 Elsevier B.V. All rights reserved.
http://dx.doi.org/10.1016/j.apcatb.2012.05.011

The disposal of chlorinated aromatic compounds is a serious environmental and social problem. Because of the high toxicity and safety concerns regarding the handling of highly chlorinated aromatics such as hexachlorobenzene (HCB), polychlorinated biphenyls (PCBs), and especially polychlorinated dibenzodioxins/polychlorinated dibenzofurans (PCDD/Fs), the degradation of lower chlorinated benzenes is usually studied as the model reaction [30–33]. 1,2,4-Trichlorobenzene (1,2,4-TrCB) is a ubiquitous environmental pollutant and has been listed as a priority pollutant in water by the US Environmental Protection Agency [34]. Because of its environmental hazards and its structural similarities to HCB, PCBs, and PCDD/Fs, 1,2,4-TrCB has often been chosen as a model compound for exploring efficient treatment technologies for chlorinated aromatics and identifying their degradation mechanisms.

Recently, metal-oxide catalysts have attracted much attention for the degradation of chlorinated aromatic compounds because of their low cost, high catalytic activity, and good thermal stability, and the ease of preparation of high-surface-area materials [35–41]. A Co–Ce composite oxide has been identified as a preferred catalyst for environmental protection. However, to the best of our knowledge, there have been no reports on the degradation of chlorinated aromatics using a Co–Ce composite oxide, especially one with a 3D hierarchical micro/nano structure.

In this paper, a 3D flower-like Co–Ce composite oxide with a micro/nano structure was synthesized using an ethylene-glycol-mediated method. The degradation of 1,2,4-TrCB as a model compound was carried out over the prepared Co–Ce composite oxide, using an on-line pulsed-flow microreactor coupled with a gas chromatography (GC) system. The catalytic performance of the composite was compared with those of quartz sand, commercial Co_3O_4, commercial CeO_2, and a commercial Co_3O_4/CeO_2 equimass mixture. The Co–Ce composite oxide showed good catalytic performance in the degradation of 1,2,4-TrCB. The cause of the high activity is attributed to the structural features of the composite oxide with a high specific surface area and a high total pore volume as well as the catalytic synergistic effect between the two composite phases. The apparent activation energy of the pulsed reaction of 1,2,4-TrCB over the 3D flower-like Co–Ce composite oxide was also calculated on the basis of pulsed catalytic theory.

2. Experimental

2.1. Preparation of flower-like Co–Ce composite oxide

In a typical procedure, 0.002 mol of cobalt nitrate ($Co(NO_3)_2{\cdot}6H_2O$), 0.002 mol of cerium nitrate ($Ce(NO_3)_3{\cdot}6H_2O$), 0.037 mol of urea, and 0.019 mol of tetrabutylammonium bromide (TBAB) were added to 150 mL of ethylene glycol (EG). The mixture was stirred with a magnetic stirring-bar and heated to 180 °C for about 35 min. The precipitated precursor was cooled to room temperature and washed three times with absolute alcohol, using centrifugation–redispersion cycles, and then calcined at 600 °C for 2 h to prepare the flower-like Co–Ce composite oxide.

2.2. Materials characterization

The products were characterized by high-resolution scanning electron microscopy (SEM; Zeiss Supra 55, Zeiss, Oberkochen, Germany), high-resolution transmission electron microscopy (TEM; JEM-2100, JEOL, Tokyo, Japan), X-ray powder diffraction (XRD; D/max 2500 diffractometer, Rigaku, Tokyo, Japan; with Cu Kα radiation, λ = 0.15418 nm), pore structure analysis using an automated surface area and pore size analyzer (QUADRASORB SI-MP, Quantachrome, Boynton Beach, FL, USA), and thermogravimetric and differential thermal analyses (TG–DTA, microcomputer differential thermal balance, Hengjiu, Beijing, China). TG–DTA experiments were performed between ambient temperature and 850 °C with a heating rate of 10 °C/min in an air flow. Elemental analysis of the Co–Ce composite oxide was performed using an Optima 2000 DV model (Perkin-Elmer, USA) inductively coupled plasma optical emission spectrometer. Sample solutions were prepared by dissolving the samples in 1 M HNO_3 aqueous solution.

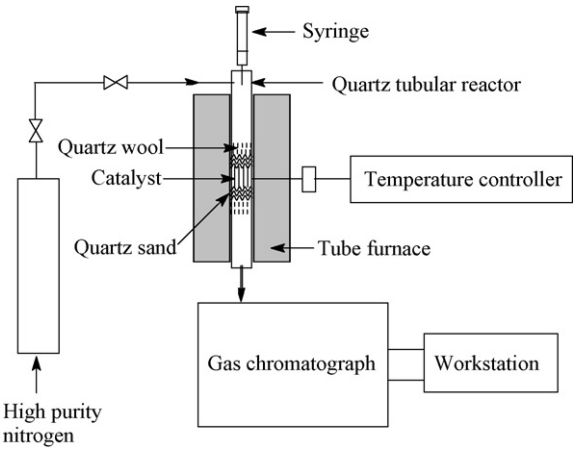

Scheme 1. Experimental apparatus of the pulsed-flow microreactor–gas chromatography system.

2.3. Electron spin resonance experiments

Superoxide anions were measured using an electron spin resonance (ESR) spectrometer (ESP 300E, Bruker, Germany) as described below. Co–Ce composite oxide (100 mg) and 1,2,4-TrCB (0.5 μL) were mixed in an ampoule, which was sealed and heated at 573 K for 5 min. The reaction products were immediately dissolved in dimethyl sulfoxide (Sigma Chemical Co., St Louis, MO, USA). The superoxide anions were characterized by ESR using 5,5-dimethyl-1-pyrroline *N*-oxide (DMPO; Sigma Chemical Co.) as a spin trapping agent. The instrument settings were microwave power 10 mW, microwave frequency 9.8 GHz, scanning range 100 G, modulation frequency 100 kHz, modulation amplitude 2 G, and sweep time 41.943 s.

2.4. Catalytic activity measurements

Catalytic activity measurements were carried out in a pulsed-flow microreactor coupled with a GC system, as illustrated in Scheme 1. A quartz tube with an inner diameter of 6 mm was chosen as the reactor tube, and the catalyst was packed between quartz sand and quartz wool in the reactor. The reactor was heated using a tube furnace and the temperature was monitored using a temperature controller equipped with a K-type thermocouple positioned in the proximity of the catalyst bed. 1,2,4-TrCB (0.5 μL) was introduced into the injection port in the upper reactor, where it immediately evaporated. The effluent gases were analyzed on-line using a gas chromatograph equipped with a flame ionization detector. The activity was expressed as the degradation efficiency (DE) of 1,2,4-TrCB, calculated by Eq. (1):

$$\mathrm{DE}(\%) = \left(1 - \frac{R_{\mathrm{TrCB}}}{I_{\mathrm{TrCB}}}\right) \times 100\% \quad (1)$$

where I_{TrCB} is the initial injection amount of 1,2,4-TrCB, and R_{TrCB} is the residual amount of 1,2,4-TrCB after the reaction.

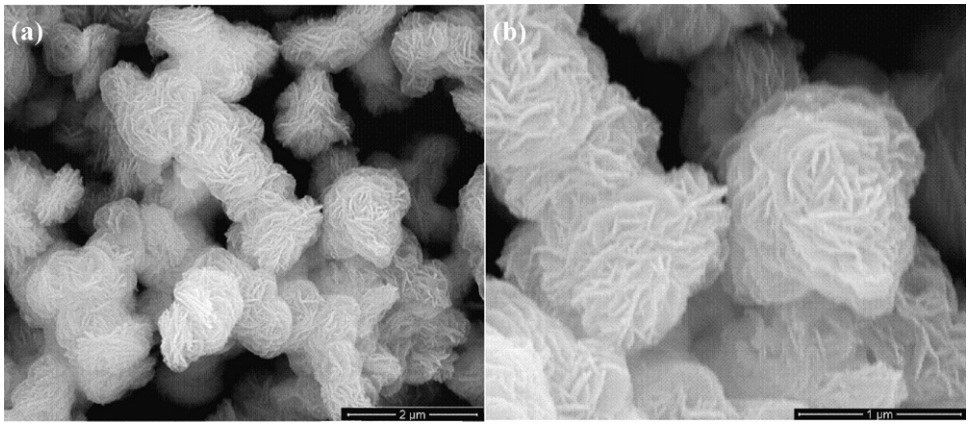

Fig. 1. (a) Low-magnification SEM image and (b) high-magnification SEM image of the Co_3O_4–CeO_2 composite oxide precursor.

3. Results and discussion

3.1. Preparation and characterization of precursor

The precursors, synthesized by the ethylene-glycol-mediated process described above, were dried in an oven at 60 °C for 6 h. Fig. 1 shows the SEM images of the prepared precursor, which was composed of uniform flower-like structures with diameters of about 1 μm. The entire hierarchical structure is built from multiple layers of nanopetals with relatively smooth surfaces, probably as a result of Ostwald ripening [24,42]. These multiple layers of nanopetals were connected to each other through the center to form 3D flower-like structures.

In order to study the formation process of the precursor, time-dependent experiments were carried out, during which precipitates were collected at different time intervals once the reaction temperature was up to 180 °C. An obvious morphology evolution process was observed. Fig. 2 shows that this morphology evolution process, controlled by time, is consistent with the so-called two-stage growth process reported for ethylene-glycol-mediated synthesis reactions [24,25,27,28,42]. In the initial stage, the cobalt and cerium nitrates coordinated with EG produced cobalt and cerium alkoxides [24,25,28], which were amorphous and precipitated quickly. Then these precipitates redissolved, renucleated, and crystallized to form multiple layers of nanopetals. These multiple layers of nanopetals assembled a hierarchical structure through a center. Later, with further growth, the amount of nanopetals increased, and a 3D flower-like hierarchical structure was formed.

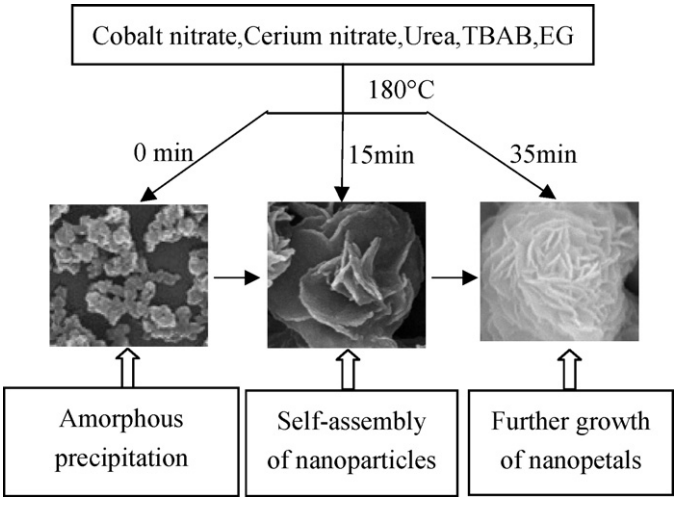

Fig. 2. Possible morphological evolution process of the precursor.

It is noteworthy that both TBAB and urea played a vital role in the synthesis of the Co–Ce composite oxide precursor. When no TBAB was added as a surfactant under the same reaction conditions, most of the nanopetals were unable to assemble into flower-like structures, as shown in Fig. S1(a). This indicates that TBAB can facilitate the assembly of petals into flower-like structures, probably through interaction of TBAB molecules with petals, similar to cases reported in the literature [25,43]. Moreover, when there was no urea in the reaction system, the precursor had an irregular compact structure instead of a loose flower-like structure, as shown in Fig. S1(b). These findings indicate that the addition of urea to the reaction system was critical for the formation of the flower-like geometry, and essentially inhibited any further agglomeration. The important roles of surfactants and urea in ethylene-glycol-mediated self-assembly processes for micro/nano materials of cerium oxide and iron oxide have been reported [24,25].

TG–DTA was performed to investigate the thermal stability of the precursor. Analysis of the thermal decomposition of the precursor was used to determine the optimum calcination temperature for producing good composite metal-oxide crystals. Fig. S2 shows the TG–DTA curve of the precursor. There are two endothermal peaks centered at about 185 °C and 260 °C, respectively, which is in agreement with two weight-loss steps. The first weight-loss is ascribed to the removal of physically adsorbed water; the second weight-loss, between 240 °C and 350 °C, is about 25.5% and represents removal of organic species in the precursor by calcination. There is almost no weight loss above 600 °C, which means that the precursors have been entirely decomposed at 600 °C.

3.2. Preparation and characterization of flower-like Co–Ce composite oxide

The target metal oxide was simply obtained by thermal treatment of the precursor [44]. Based on the TG–DTA results shown in Fig. S2, the precursor was calcined at 600 °C for 2 h in a muffle furnace to obtain the Co–Ce composite oxide. The large-scale SEM image of the calcined product shown in Fig. 3(a) reveals that the calcination had no obvious effect on the overall morphology, and the construction units are still 3D flower-like composite structures assembled in multiple layers. However, the high-magnification SEM image in Fig. 3(b) shows that the surfaces of the petals in the flower-like structures were no longer smooth, probably as a result of the removal of organic species [24]. After calcination, each petal of the flower-like structure had been transformed into a highly porous structure consisting of interconnected nanoparticles.

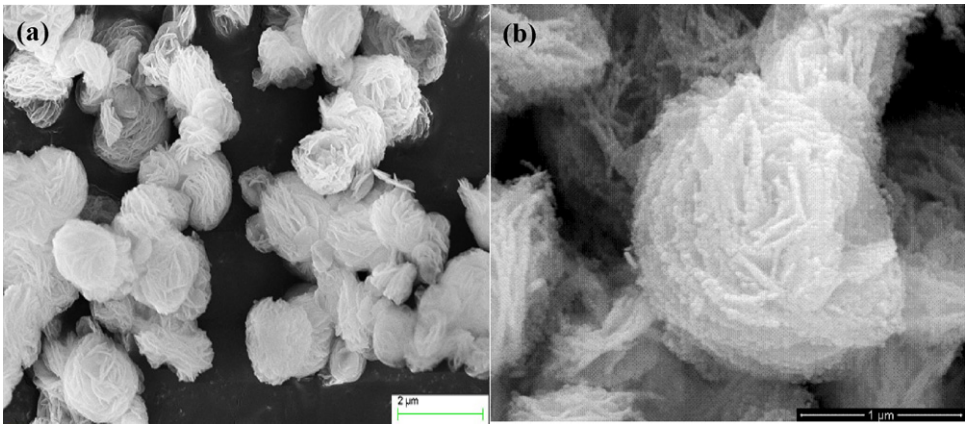

Fig. 3. (a) Low-magnification SEM image and (b) high-magnification SEM image of the flower-like Co_3O_4–CeO_2 composite oxide.

The sizes of these nanoparticles were in the range 10–15 nm. The TEM images shown in Fig. 4 further verified that this flower-like structure was highly porous and consisted of many interconnected nanoparticles, and the whole structure was on the micrometer scale. The results verified that the flower-like Co–Ce composite oxide is a type of micro/nano material, possessing the advantages of both microstructures and nanostructures. A high-magnification TEM image taken from the flower-like building block, shown in Fig. 4(c), reveals that the lattice fringes are clearly visible with a spacing of 0.31 nm, which is in good agreement with the spacing of the (1 1 1) planes of CeO_2 [13,24]. Selected area electron diffraction analysis (Fig. 4(d)) shows diffraction rings, which indicates the highly polycrystalline nature of these materials [25,27]. The XRD patterns in Fig. 5 reveal that all the reflections belong to pure cobalt oxide (JCPDS 01-080-1541) [10] and pure cubic fluorite-structured cerium oxide (JCPDS 00-034-0394) [10]. Energy-dispersive X-ray spectroscopy (Fig. S3) verified that the prepared flower-like Co–Ce composite oxide consisted of Co, Ce, and O, which agreed well with a Co–Ce composite oxide, and the distributions of Co, Ce, and O on the surface of the material were relatively homogeneous. The elemental analysis results show that the Ce/Co atomic ratio in the Co–Ce composite oxide is about 5:1.

Fig. S4 shows the N_2 adsorption–desorption isotherms and Barrett–Joyner–Halenda pore size distribution of the Co–Ce composite oxide. The results show that the flower-like Co–Ce composite oxide exhibits typical IV-shaped isotherms [6], which is

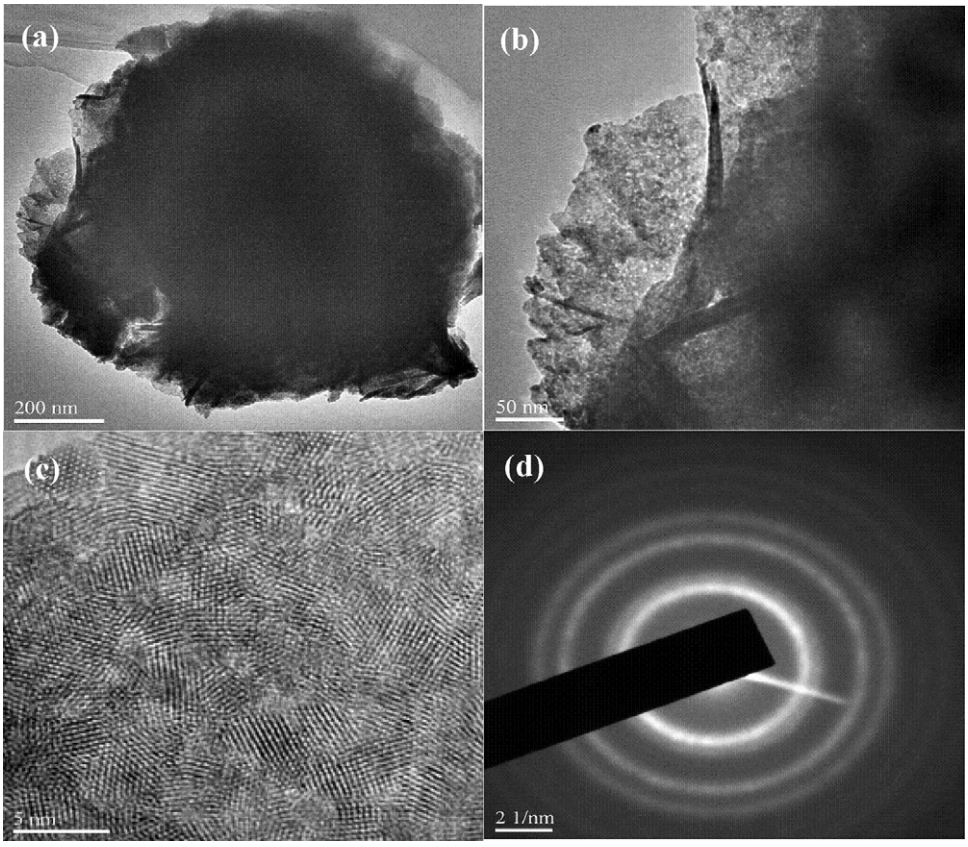

Fig. 4. (a) and (b) TEM images of the flower-like Co_3O_4–CeO_2 composite oxide; (c) high-magnification TEM image of the flower-like Co_3O_4–CeO_2 composite oxide; and (d) selected area electron diffraction pattern of the flower-like Co_3O_4–CeO_2 composite oxide.

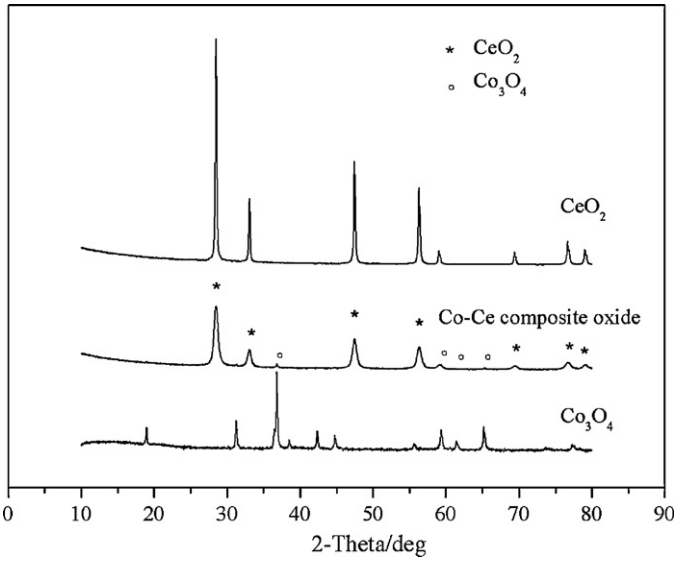

Fig. 5. XRD patterns of various materials.

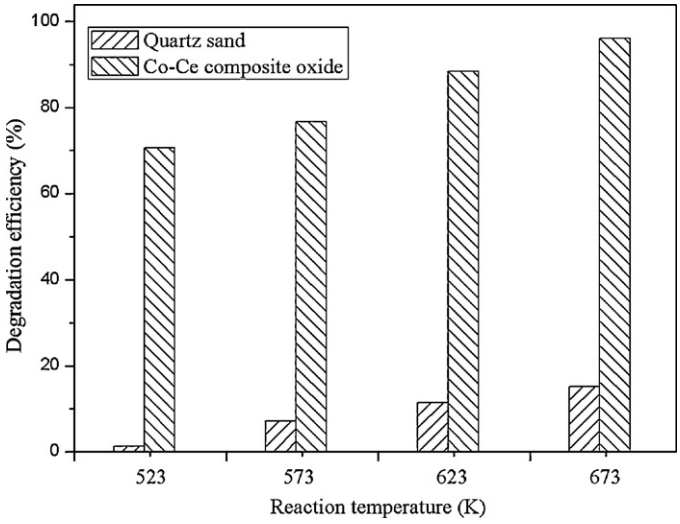

Fig. 6. Effects of reaction temperature on the degradation of 1,2,4-TrCB.

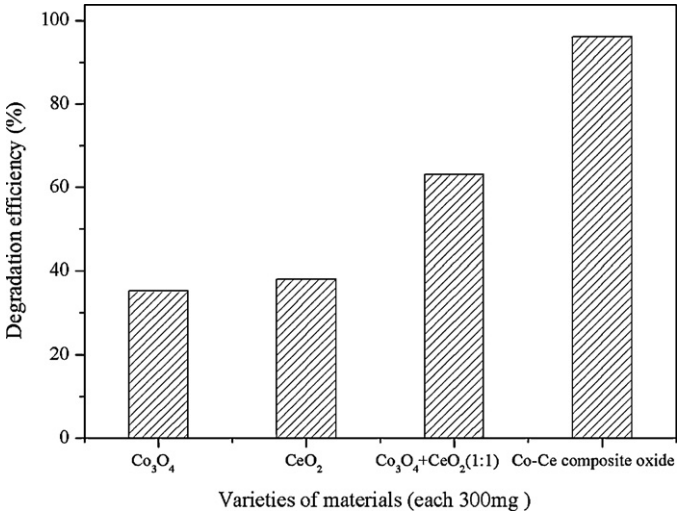

Fig. 7. Effects of various materials on the degradation of 1,2,4-TrCB.

characteristic of mesoporous materials. In the first stage, the adsorbance rises more slowly with increasing relative pressure (P/P_0), and adsorption condensation occurs at the surface of the pore wall. As P/P_0 continues to increase, capillary condensation of N_2 occurs in the pores, and the isotherms appear as a type H3 hysteresis loop, based on the IUPAC system [45]. This type of hysteresis phenomenon often occurs in congeries or agglomerates of particles with slit-type pores [23]. The appearance of a hysteresis loop indicates that the sizes and shapes of the pores are relatively uniform. The pore size distribution of the Co–Ce composite oxide, shown in Fig. S4(b), indicates that this material has a narrow pore size distribution with a maximum centered at about 8 nm, an average pore diameter of 8.8 nm, a Brunauer–Emmett–Teller (BET) surface area of 42 m^2/g, and a total pore volume of 0.090 cm^3/g.

3.3. Catalytic activity measurements

The combination of a pulsed-flow microreactor coupled with a GC system is widely used in the petrochemical industry for evaluation and selection of cracking catalysts, and investigation of reaction mechanisms and kinetics. This technique has the advantages of short reaction times and low reactant dosages [46–48]. However, this method has seldom been used for evaluating and selecting catalysts for degradation of chlorinated aromatic compounds. In this study, the degradation of 0.5 μL of 1,2,4-TrCB was carried out over the Co–Ce composite oxide (each 300 mg) using an on-line pulsed-flow microreactor–GC system. The catalytic performance of the composite oxide was compared with those of quartz sand, commercial Co_3O_4, commercial CeO_2, and a commercial Co_3O_4/CeO_2 equimass mixture.

Fig. 6 shows the temperature-dependent degradation efficiency of 1,2,4-TrCB on the flower-like Co–Ce composite oxide and quartz sand, the latter being in the absence of the catalyst. It can be seen that only a little 1,2,4-TrCB was degraded on the quartz sand at 523 K. The degradation efficiency increased very slowly with increasing reaction temperature and reached only about 15% at 673 K. Quartz sand, therefore, seems to have very low activity in the degradation of 1,2,4-TrCB. In contrast, the degradation efficiency of 1,2,4-TrCB on the flower-like Co–Ce composite oxide was much higher than that on the quartz sand at the corresponding reaction temperatures. At a reaction temperature of 673 K, the degradation efficiency was up to 96% in a very short reaction time. This indicates that the Co–Ce composite oxide gave a better catalytic performance in the degradation of 1,2,4-TrCB.

The reactivity of the Co–Ce composite oxide in the degradation of 1,2,4-TrCB was further compared with that of commercial Co_3O_4, commercial CeO_2, and a Co_3O_4/CeO_2 equimass mixture. As shown in Fig. 7, the degradation efficiency of 1,2,4-TrCB on the Co–Ce composite oxide was also higher than those over the equimass mixture, pure commercial CeO_2, and pure commercial Co_3O_4. This further demonstrated the superior performance of the Co–Ce composite oxide as a catalyst in the degradation of 1,2,4-TrCB.

The properties of catalysts are strongly dependent on the surface active sites, which are determined by structural properties such as surface area and pore volume [23]. Table 1 lists the pore structure data of different materials. Obviously, the specific surface area

Table 1
Pore structure data of different materials.

Materials	S_{BET} (m^2/g)	Total pore volume (cm^3/g)	Average pore diameter (nm)
Commercial Co_3O_4	4	0.043	31.1
Commercial CeO_2	6	0.034	23.6
Co–Ce composite oxide	42	0.090	8.8

and total pore volume of the flower-like Co–Ce composite oxide are larger than those of commercial Co_3O_4 and commercial CeO_2, leading to more surface active sites. These might contribute to the superior performance of the Co–Ce composite oxide in the degradation of 1,2,4-TrCB. A similar case concerning the increase in activity caused by a large increase in specific surface area has been reported by Wang et al. [49] for the degradation of trichloroethylene on CeO_2 calcined at different temperatures.

Another interesting finding is that the degradation efficiency of 1,2,4-TrCB over the Co_3O_4/CeO_2 equimass mixture is higher than that over pure commercial CeO_2 or pure commercial Co_3O_4, as shown in Fig. 7. This implies that the mixture of commercial Co_3O_4 and commercial CeO_2 had a synergistic effect in the degradation of 1,2,4-TrCB. From this result, it can be postulated that the Co–Ce composite oxide also has a synergistic effect in the degradation of 1,2,4-TrCB. A similar catalytic synergistic effect over a Co_3O_4/CeO_2 composite oxide has been reported in methane oxidation [9], N_2O decomposition [10], diesel-soot oxidation [11], and low-temperature CO oxidation [8,12,13]. It has been verified that CeO_2 has high oxygen-storage and oxygen-transport capacities, and well-known catalytic and redox properties, making more oxygen available for oxidation processes [12]. Combining CeO_2 with other metal oxides often affects the mobility of oxygen on their surfaces. By providing oxygen to or withdrawing oxygen from other elements, CeO_2 can affect the oxidation states of elements combined with it. The redox ability and catalytic performance of these elements can be effectively modified by CeO_2 [10,50]. The ease with which CeO_2 adsorbs oxygen from the gas phase and transports it to other catalyst components is the reason why it is added to other oxidation catalysts [51]. In our former study [52], it was found that cabbage-like Co_3O_4 materials showed high reactivity in the degradation of 1,2,4-TrCB. The degradation of 1,2,4-TrCB on the cabbage-like Co_3O_4 is hypothesized to act competitively via hydrodechlorination and oxygen-attacking pathways. In the hydrodechlorination pathway, 1,2,4-TrCB is successively dechlorinated into the three dichlorobenzenes, and then monochlorobenzene. On the other hand, the lattice oxygen and superoxide anions in this material may take part in oxidation reactions, which oxidize 1,2,4-TrCB to chlorophenol and dichlorophenol, and even CO_2 and H_2O. To identify whether $O_2^{-\bullet}$ participated in the degradation of 1,2,4-TrCB on the Co–Ce composite oxide, ESR analysis was used to obtain information about the superoxide anions. The results are shown in Fig. S5. The characteristic peaks of $O_2^{-\bullet}$ were observed, and the hyperfine constants, $\alpha_N = 13.6$ G and $g = 2.0097$, coincided with those identified previously as DMPO-$O_2^{-\bullet}$ [53]. The ESR results shown in Fig. S5 confirmed the existence of the superoxide anion, which may be involved in the degradation of 1,2,4-TrCB, causing the ring-cracking oxidation of 1,2,4-TrCB to smaller molecular intermediates, and perhaps even to CO_2 and H_2O.

Fig. 8 showed the chromatogram of the degradation products of 0.5 μL of 1,2,4-TrCB on commercial Co_3O_4, commercial CeO_2, a Co_3O_4/CeO_2 equimass mixture, and the Co–Ce composite oxide (each 300 mg) at 673 K, respectively. Peaks 1–4 were identified as *m*-dichlorobenzene, *p*-dichlorobenzene, *o*-dichlorobenzene, and the unreacted 1,2,4-TrCB, respectively. In comparison, over the Co–Ce composite oxide, the unreacted 1,2,4-TrCB was the smallest, and the amounts of dichlorobenzenes produced via hydrodechlorination were the smallest, too. This means that the Co–Ce composite oxide was the optimal catalyst for the competitive oxidative reaction of 1,2,4-TrCB as a result of the interaction of the two components. When Co_3O_4 was combined with CeO_2 in a flower-like Co–Ce composite oxide, the Co–Ce composite oxide showed a synergistic interaction in the degradation of 1,2,4-TrCB. One possible reason is that the Co—O bond at the cerium oxide and cobalt oxide boundary is elongated, and breaks more easily [13,46]. As a result

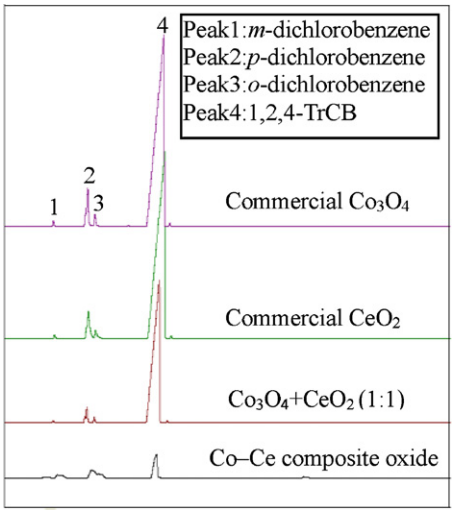

Fig. 8. Chromatogram of degradation products of 0.5 μL of 1,2,4-TrCB on different materials (each 300 mg) at 673 K.

of the interaction of the two components, the lattice oxygen and superoxide anions escape from Co_3O_4 more easily. The other possibility is that oxygen on CeO_2 could be quickly transported via oxygen vacancies to the surface of Co_3O_4, once the lattice oxygen and superoxide anions of Co_3O_4 were consumed. The oxygen transported from CeO_2 would greatly promote the oxidizability of Co_3O_4 in the degradation of 1,2,4-TrCB. Based on the degradation mechanism of 1,2,4-TrCB on cabbage-like Co_3O_4 materials [52], a possible synergistic degradation pathway of the Co–Ce composite oxide is shown in Fig. 9.

3.4. Kinetic study of pulsed reactions

Under pulsed conditions, the mass ratio of catalysts to 1,2,4-TrCB is very high, and the retention time of the reactant on the catalyst surface is very short. The catalysts, therefore, have sufficient surface area for the adsorption of reactants, and competitive adsorption between reactants and products can be ignored. In order to investigate the kinetics of pulsed reactions, the effects of the dosage of the flower-like Co–Ce composite oxide on the degradation of 1,2,4-TrCB at 573 K and 673 K were studied, where the amount of 1,2,4-TrCB was fixed at 0.5 μL. The results are shown in Fig. S6.

It can be seen from Fig. S6 that with increasing dosage of the flower-like Co–Ce composite oxide, the degradation of 1,2,4-TrCB increased greatly, at both 573 K and 673 K. Regression of $\ln[1/(1-x)]$ versus the dosage of the flower-like Co–Ce composite oxide is nearly linear, as shown in Fig. 10. This indicates that degradation of 1,2,4-TrCB on the composite basically conforms to first-order kinetics, i.e., the kinetic behavior can be described by a first-order reaction kinetics model.

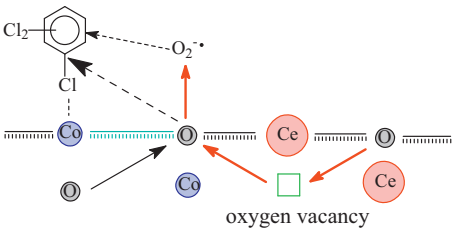

Fig. 9. Proposed synergistic degradation mechanism of 1,2,4-TrCB on the flower-like Co_3O_4–CeO_2 composite oxide.

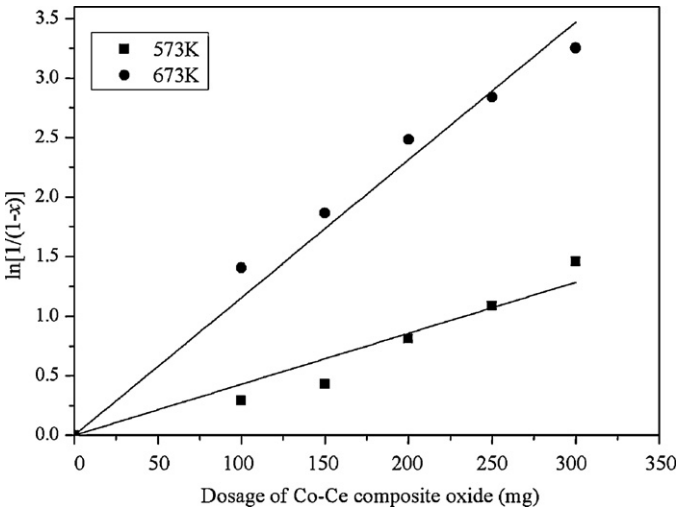

Fig. 10. Plot of $\ln[1/(1-x)]$ versus dosage of the flower-like Co_3O_4–CeO_2 composite oxide.

The pulsed-flow microreactor–gas chromatographic method can permit a simple quantitative study of first-order reactions, because the fractional conversion of reactants to products is independent of pressure for a first-order reaction, and the rate of adsorption must be faster than the rate of the surface reaction for the latter to be the rate-controlling step. The quantitative treatment also assumes that the adsorption isotherm is basically linear [54]. According to these conditions and hypotheses, Bassett and Habgood [54] deduced that the first-order kinetics of the pulsed catalytic chromatograph is as shown in Eq. (2):

$$k_{obv} = \frac{F_c}{RTW} \ln\left(\frac{1}{1-x}\right) \quad (2)$$

where k_{obv} represents the apparent rate constant, mol/(kg Pa s); F_c is the flow velocity, m^3/s; T represents the reaction temperature, K; W is the dosage of catalyst, kg; R is the gas constant, 8.315 J/(K mol); and x is the degradation efficiency, %.

From Eq. (2), the apparent rate constants of 1,2,4-TrCB degradation at 573 K and 673 K are $k_{obv1} = 0.4502 \times 10^{-6}$ mol/(kg Pa s) and $k_{obv2} = 1.0333 \times 10^{-6}$ mol/(kg Pa s), respectively.

Furthermore, according to the Arrhenius equation (Eq. (3)), the apparent activation energy of the degradation on the Co–Ce composite oxide was calculated to be about 27 kJ/mol, whereas the apparent activation energy of the degradation on a Co_3O_4/CeO_2 equimass mixture was about 32 kJ/mol under the same conditions (the related results and calculation are shown in Supplement Materials). The apparent activation energy is less than those reported for dechlorination of tetrachloroethylene by nanoscale Pd/Fe and Fe particles (31.1 and 44.9 kJ/mol, respectively) [55], and the gas phase hydrodechlorination of chlorobenzene (61 ± 3 kJ/mol), 1,2-dichlorobenzene (84 ± 3 kJ/mol) and 1,4-dichlorobenzene (98 ± 4 kJ/mol) over supported nickel in the temperature range 473–573 K [56]. The apparent activation energy of the degradation of 1,2,4-TrCB on the Co–Ce composite oxide is also as low as those reported for the catalytic ozonation of chlorobenzene over iron oxide and manganese oxide catalysts (20–48 kJ/mol) in the temperature range 303–523 K [57], for the catalytic oxidation of 1,2-dichlorobenzene over a series of V_2O_5/TiO_2-based catalysts (29–37 kJ/mol) in the temperature range 473–673 K [58], and for catalytic oxidation of 1,2-dichlorobenzene at temperature higher than 673 K over V_2O_5/TiO_2 and V_2O_5/MoO_3–TiO_2 (34.4 kJ/mol and 31.5 kJ/mol, respectively) [59]. Those comparisons demonstrated the good performance of the Co–Ce composite oxide in the degradation of 1,2,4-TrCB. Recently, the application of various modifications such as MnO_2 and ZrO_2 to increase the reactivity of CeO_2 in the degradation of chlorinated organic compounds has been widely investigated [32,60–65]. Wang et al. [60–62] have studied the catalytic combustion of chlorobenzene over various modified CeO_2 catalysts; most of the modified catalysts showed good performances in the catalytic combustion of chlorobenzene. Gutiérrez-Ortiz et al. [63] have also found that ZrO_2/CeO_2 catalysts exhibited adequate catalytic performance for gas-phase oxidation of 1,2-dichloroethane. The present study and the results that have already been reported show that the good performances of these catalysts may be attributed to the superior properties of multicomponent materials, including the interactions of different components, and the high oxygen mobilities of the materials.

$$\ln\frac{k_1}{k_2} = \frac{E_a}{R}\left(\frac{1}{T_2} - \frac{1}{T_1}\right) \quad (3)$$

where k_1 and k_2 are the apparent rate constants at 573 K and 673 K, respectively, mol/(kg Pa s); E_a is the apparent activation energy, kJ/mol; and T_1 and T_2 are the reaction temperatures, K.

4. Conclusions

An ethylene-glycol-mediated process was used to synthesize a micrometer-sized, nanostructured, flower-like Co–Ce composite oxide. The precursor was formed in two stages, during which TBAB facilitated the assembly of petals into flower-like structures, and urea was critical for flower formation and inhibited further agglomeration. The Co–Ce composite oxide was obtained from the precursor by calcination. The composite oxide was assembled from polycrystalline nanoparticles, with large surface areas and typical mesoporous structures.

Catalytic activity measurements using a pulsed-flow microreactor–GC system showed that the composite oxide had better activity in 1,2,4-TrCB degradation than did various commercial materials. The high activity was attributed to the structural features of the composite oxide with a high specific surface area and a high total pore volume as well as the synergistic catalytic effects between the two phases of the composite.

Pulsed catalytic theory suggests that reaction of the composite oxide with 1,2,4-TrCB is approximately first-order. The apparent activation energy was lower than that of a Co_3O_4/CeO_2 equimass mixture, indicating easy degradation as a result of the catalytic effects of the composite oxide.

Acknowledgments

This study was supported by the Chinese Academy of Sciences (Grant No. KZCX2-YW-QN407), the National 973 program (2009CB421606), the National Natural Science Foundation of China (51078346, 21177141, 20807049, 21077121), and Youth Innovation Promotion Association, CAS.

Appendix A. Supplementary data

Supplementary data associated with this article can be found, in the online version, at http://dx.doi.org/10.1016/j.apcatb.2012.05.011.

References

[1] Y.J. Mergler, J. Hoebink, B.E. Nieuwenhuys, Journal of Catalysis 167 (1997) 305–313.
[2] J. Jansson, Journal of Catalysis 194 (2000) 55–60.
[3] K. Asano, C. Ohnishi, S. Iwamoto, Y. Shioya, M. Inoue, Applied Catalysis B 78 (2008) 242–249.

[4] W. Piskorz, F. Zasada, P. Stelmachowski, A. Kotarba, Z. Sojka, Catalysis Today 137 (2008) 418–422.
[5] T.L. Lai, Y.L. Lai, C.C. Lee, Y.Y. Shu, C.B. Wang, Catalysis Today 131 (2008) 105–110.
[6] T. Tsoncheva, L. Ivanova, C. Minchev, M. Fröba, Journal of Colloid and Interface Science 333 (2009) 277–284.
[7] M.K. Jia, G.J. Su, M.H. Zheng, B. Zhang, S.J. Lin, Science China Chemistry 53 (2010) 1266–1272.
[8] C.W. Tang, M.C. Kuo, C.J. Lin, C.B. Wang, S.H. Chien, Catalysis Today 131 (2008) 520–525.
[9] L.F. Liotta, G. Di Carlo, G. Pantaleo, A.M. Venezia, G. Deganello, Applied Catalysis B 66 (2006) 217–227.
[10] L. Xue, C.B. Zhang, H. He, Y. Teraoka, Applied Catalysis B 75 (2007) 167–174.
[11] M. Dhakad, T. Mitshuhashi, S. Rayalu, P. Doggali, S. Bakardjiva, J. Subrt, D. Fino, H. Haneda, N. Labhsetwar, Catalysis Today 132 (2008) 188–193.
[12] C.W. Tang, C.C. Kuo, M.C. Kuo, C.B. Wang, S.H. Chien, Applied Catalysis A 309 (2006) 37–43.
[13] J.Y. Luo, M. Meng, X. Li, X.G. Li, Y.Q. Zha, T.D. Hu, Y.N. Xie, J. Zhang, Journal of Catalysis 254 (2008) 310–324.
[14] S. Kannan, C.S. Swamy, Catalysis Today 53 (1999) 725–737.
[15] J.J. Wei, Z.J. Yang, H.X. Yang, T. Sun, Y.Z. Yang, Crystengcomm 13 (2011) 4950–4955.
[16] D.P. Dutta, N. Manoj, A.K. Tyagi, Journal of Luminescence 131 (2011) 1807–1812.
[17] D.M. Kempaiah, S. Yin, T. Sato, Crystengcomm 13 (2011) 741–746.
[18] H.F. Li, G.Z. Lu, Y.Q. Wang, Y. Guo, Y.L. Guo, Catalysis Communications 11 (2010) 946–950.
[19] E. Moretti, L. Storaro, A. Talon, M. Lenarda, P. Riello, R. Frattini, M.V.M. de Yuso, A. Jimenez-Lopez, E. Rodriguez-Castellon, F. Ternero, A. Caballero, J.P. Holgado, Applied Catalysis B 102 (2011) 627–637.
[20] J.P. Cheng, X. Chen, R. Ma, F. Liu, X.B. Zhang, Materials Characterization 62 (2011) 775–780.
[21] M.Y. Wang, D.G. Zhang, Z.W. Tong, W.X. Ma, X.Y. Xu, Micro & Nano Letters 5 (2010) 207–210.
[22] Z.P. Chen, A.Q. Xu, Y. Zhang, N. Gu, Current Applied Physics 10 (2010) 967–970.
[23] M.K. Jia, G.J. Su, M.H. Zheng, B. Zhang, S.J. Lin, Journal of Nanoscience and Nanotechnology 11 (2011) 2100–2106.
[24] L.S. Zhong, J.S. Hu, H.P. Liang, A.M. Cao, W.G. Song, L.J. Wan, Advanced Materials 18 (2006) 2426–2431.
[25] L.S. Zhong, J.S. Hu, A.M. Cao, Q. Liu, W.G. Song, L.J. Wan, Chemistry of Materials 19 (2007) 1648–1655.
[26] A.M. Cao, J.D. Monnell, C. Matranga, J.M. Wu, L.L. Cao, D. Gao, Journal of Physical Chemistry C 111 (2007) 18624–18628.
[27] S.W. Bain, Z. Ma, Z.M. Cui, L.S. Zhang, F. Niu, W.G. Song, Journal of Physical Chemistry C 112 (2008) 11340–11344.
[28] A.M. Cao, J.S. Hu, H.P. Liang, W.G. Song, L.J. Wan, X.L. He, X.G. Gao, S.H. Xia, Journal of Physical Chemistry B 110 (2006) 15858–15863.
[29] N. Chakroune, G. Viau, S. Ammar, N. Jouini, P. Gredin, M.J. Vaulay, F. Fievet, New Journal of Chemistry 29 (2005) 355–361.
[30] W.H. Wu, J. Xu, R. Ohnishi, Applied Catalysis B 60 (2005) 129–137.
[31] C.E. Hetrick, J. Lichtenberger, M.D. Amiridis, Applied Catalysis B 77 (2008) 255–263.
[32] K. Abbas, A.N. Aysha, Applied Catalysis B 80 (2008) 176–184.
[33] S. Lomnicki, J. Lichtenberger, Z.T. Xu, M. Waters, J. Kosman, M.D. Amiridis, Applied Catalysis B 46 (2003) 105–119.
[34] D. Jaime, R. Manuel, D. Mario, Water, Air, and Soil Pollution 177 (2006) 3–17.
[35] A.K. Hall, J.M. Harrowfield, R.J. Hart, P.G. McCormick, Environmental Science and Technology 30 (1996) 3401–3407.
[36] D.F. Ollis, E. Pelizzetti, N. Serpone, Environmental Science and Technology 25 (1991) 1522–1529.
[37] G.A. Zacheis, K.A. Gray, P.V. Kamat, Journal of Physical Chemistry B 105 (2001) 4715–4720.
[38] T. Öberg, B. Bergbäck, M. Filipsson, Chemosphere 71 (2008) 1135–1143.
[39] J. Lichtenberger, M.D. Amiridis, Journal of Catalysis 223 (2004) 296–308.
[40] G. Schetter, R. Horch, H. Stuetzle, B.H. Hagenmaie, Organohalogen Compounds 3 (1990) 165–168.
[41] X. Zhang, P.E. Savage, Catalysis Today 40 (1998) 333–342.
[42] Y. Cheng, Y.S. Wang, Y.H. Zheng, Y. Qin, Journal of Physical Chemistry B 109 (2005) 11548–11551.
[43] H. Cölfen, M. Antonietti, Angewandte Chemie International Edition 44 (2005) 5576–5591.
[44] D. Larcher, G. Sudant, R. Patrice, J.M. Tarascon, Chemistry of Materials 15 (2003) 3543–3551.
[45] J. Rouquerol, D. Avnir, C.W. Fairbridge, D.H. Everett, J.H. Haynes, N. Pernicone, J.D.F. Ramsay, K.S.W. Sing, K.K. Unger, Pure and Applied Chemistry 66 (1994) 1739–1758.
[46] D.B. Dadyburjor, Z.Y. Liu, Journal of Catalysis 141 (1993) 148–160.
[47] P.M. Michalakos, R.C. Robinson, Y. Tang, Catalysis Today 46 (1998) 13–26.
[48] J.W. Dean, D.B. Dadyburjor, Industrial and Engineering Chemistry Research 27 (1988) 1754–1759.
[49] Q.G. Dai, X.Y. Wang, G.Z. Lu, Applied Catalysis B 81 (2008) 192–202.
[50] S. Imamura, M. Shono, N. Okamoto, A. Hamada, S. Ishida, Applied Catalysis A 142 (1996) 279–288.
[51] E. Iwanek, K. Krawczyk, J. Petryk, J.W. Sobczak, Z. Kaszkur, Applied Catalysis B 106 (2011) 416–422.
[52] S.J. Lin, G.J. Su, M.H. Zheng, M.K. Jia, C.S. Qi, W. Li, Journal of Hazardous Materials 192 (2011) 1697–1704.
[53] L.Y. Zang, K. Stone, W.A. Pryor, Free Radical Biology and Medicine 19 (1995) 161–167.
[54] D.W. Bassett, H.W. Habgood, Journal of Physical Chemistry 64 (1960) 769–773.
[55] H.L. Lien, W.X. Zhang, Applied Catalysis B 77 (2007) 110–116.
[56] M.A. Keane, G. Pina, G. Tavoularis, Applied Catalysis B 48 (2004) 275–286.
[57] H.C. Wang, H.S. Liang, M.B. Chang, Journal of Hazardous Materials 186 (2011) 1781–1787.
[58] S. Krishnamoorthy, J.P. Baker, M.D. Amiridis, Catalysis Today 40 (1998) 39–46.
[59] H.Y. Chang, S.P. Wang, J.R. Chang, H.S. Sheu, S.G. Shyu, Applied Catalysis B 111–112 (2012) 476–484.
[60] X.Y. Wang, Q. Kang, D. Li, Applied Catalysis B 86 (2009) 166–175.
[61] X.Y. Wang, Q. Kang, D. Li, Catalysis Communications 9 (2008) 2158–2162.
[62] M. Wu, X.Y. Wang, Q.G. Dai, Y.X. Gu, D. Li, Catalysis Today 158 (2010) 336–342.
[63] B. de Rivas, R. Lopez-Fonseca, M.A. Gutiérrez-Ortiz, J.I. Gutierrez-Ortiz, Applied Catalysis B 104 (2011) 373–381.
[64] H.F. Li, G.Z. Lu, Q.G. Dai, Y.Q. Wang, Y. Guo, Y.L. Guo, Applied Catalysis B 102 (2011) 475–483.
[65] Y. Dai, X.Y. Wang, Q.G. Dai, D. Li, Applied Catalysis B 111–112 (2012) 141–149.